Letter

High-speed NMR imaging of capillary action in thin nontransparent porous media

R. Nicasy,[1] H. P. Huinink,[1,*] S. J. F. Erich,[1,2] and O. C. G. Adan[1,2]

[1]*Eindhoven University of Technology, Applied Physics Department, P.O. Box 513, 5600 MB Eindhoven, The Netherlands*

[2]*Organization of Applied Scientific Research, TNO The Netherlands, P.O. Box 49, 2600 AA Delft, The Netherlands*

(Received 4 May 2021; revised 12 July 2021; accepted 22 September 2021; published 19 October 2021)

An improved high-speed NMR profiling method is introduced that enables us to measure capillary action in thin, nontransparent porous media. Liquid profiles can be measured as fast as 10 ms with a spatial resolution of 14.5 μm. Capillary absorption of microliter-sized droplets into nontransparent nylon-6,6 porous membranes was studied. In nylon-6,6 sharp fronts obeying a one-dimensional Darcy model were observed. In paper the uptake did not follow this model: retardation in uptake, broader fluid fronts, and swelling was observed. These measurements nicely demonstrate the possibilities and versatility of the developed method.

DOI: 10.1103/PhysRevE.104.L043101

Fast capillary imbibition processes of liquids into thin porous media are widely studied due to the occurrence in many applications, including printing [1], porous coatings [2], filtration [3], and cooling of microelectronics [4,5]. These imbibition processes are often described with a combination of Washburn [6] and Darcy's law [7,8]. Over the years, many theoretical studies tried to extend these fundamental relations to special cases like swellable media [9,10] and imbibition of liquid droplets [11]. Obtaining experimental verification of these models is still challenging as it faces short time scales and high resolution to capture these processes. For example, the penetration of an ink droplet in paper happens at micrometer scale during the first 30–100 ms [1]. Furthermore, most of these processes happen in nontransparent media like paper or polymers. Common measuring techniques are not able to deal with these requirements coherently. Measurement techniques like optical microscopy cannot access fluids in nontransparent media, which limits their application. Automatic scanning absorptometer (ASA) [8] or weight measurements [12] are able to measure global properties like mass uptake on time scales of 10 ms, but do not give access to the liquid distribution inside the porous media. Depth information is crucial for validating Washburn and Darcy models of adsorption. More importantly, density profiles during more complex processes may provide information about swelling, front broadening, front splitting, particles motion, etc., and could not be probed at this time and length scale before. Nuclear magnetic resonance (NMR) on the other hand is able to extract liquid profiles, inside nontransparent porous media [13] with high resolution. However, NMR is a relatively slow technique due to its poor signal-to-noise ratio. Conventional NMR techniques cannot access the time scale and resolution needed for capillary action in thin porous media. In this Letter, we demonstrate high-speed NMR to visualize liquid profiles inside thin porous media (100–200 μm) with a spatial resolution of 14.5 μm and a time resolution of 10 ms. Here we report liquid distribution profiles in nontransparent thin porous layers during fast imbibition. The obtained liquid profiles are used to study liquid fronts in time for different liquid mixtures inside different porous media. Finally, the technique is used to demonstrate its potential by performing capillary imbibition in printing paper. The measured liquid profiles reveal a change in sharpness of the wetting front, retardation in uptake, combined with swelling of the substrate.

The NMR measurements were performed using a GARField ^{1}H NMR [14], designed with special poles to generate a magnetic field of 1.46 T with a gradient (G) of 40.3 [T/m]. Signals were acquired using the following pulse sequence $(90^\circ_x - \tau - [90^\circ_y - \tau - (\text{echo}) - \tau - 90^\circ_{-y} - \tau - (-\text{echo}) - \tau]_n)$, which is a modification of the well known Ostroff-Waugh sequence [15]. The difference is inserting a 90°_{-y} pulse to remove the constant background signal, which after the Fourier transform would give a peak at 0 KHz, by generating alternating positive and negative echo's which after addition will cancel out this constant background. The echo time $t_e = 2\tau$ is equal to 50 μs with an acquisition time (t_a) of 40 μs from which the theoretical resolution can be calculated with $\Delta x = 1/t_a \gamma G = 14.5$ μm [16], where the gyromagnetic ratio of water was used ($\gamma = 42.58$ MHz/T). The solid-state echo is preferred above the more widely used Carr-Purcell-Meiboom-Gill (CPMG) sequence because it only uses 90°_{-y} pulses. A CPMG sequence will use both 90° and 180° pulses that will excite slightly different regions because the excitation bandwidth will depend on the type of pulse (length and power) [17]. The use of only one type of pulse (90°) ensures to have always the same excitation profile. Because all hydrogen nuclei have a small magnetic moment, the signal will be linear dependent on the hydrogen content. Between two measurements, the delay time is set larger then 3 times T_1 to ensure 95% signal restoration. Because some penetration experiments take only 100 ms, measurement speed is the most important factor. Therefore, 3 times T_1 was chosen above the more conventional 5 times T_1 which only reduces signal

*Author to whom correspondence should be addressed: h.p.huinink@tue.nl

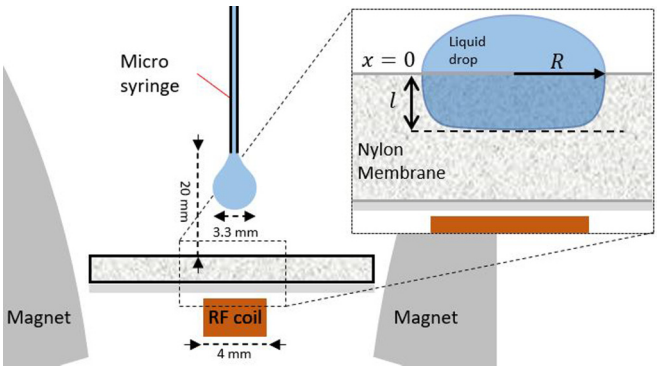

FIG. 1. Schematic representation of the measurement setup.

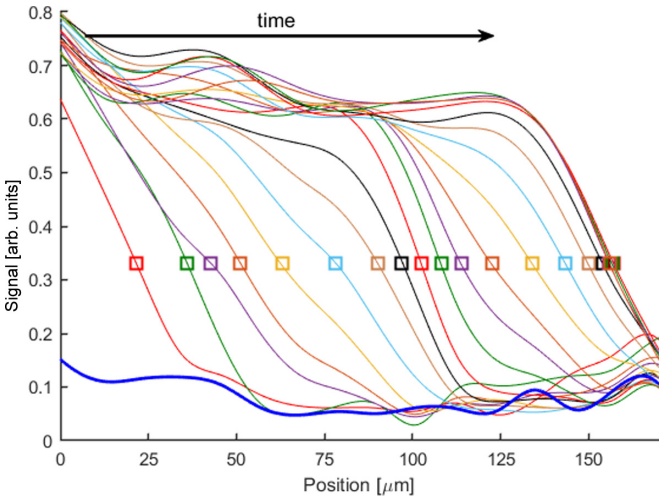

FIG. 2. Liquid profiles measured by GARField ^{1}H NMR of a 50-wt % glycerol mixture inside a 0.42-μm pore diameter nylon membrane. Profiles are measured every 25 ms and the top of the nylon membrane is set to the 0 position. The squares mark the fluid front positions. In blue, the signal acquired just before the droplet hits the sample surface is shown.

recovery from 99% ($5T_1$) to 95% ($3T_1$) but halves the measurement time. To be able to reduce this delay time, 0.1-M $CuSO_4$ was added to the liquid mixtures to lower the corresponding $T1$ times. Depending on the time scale of the imbibition process, the delay time used in our experiments was set between 10 and 50 ms. The final hydrogen profiles are obtained by adding the first 16 even positive echoes and subtracting the first 16 odd negative echoes ($n = 16$) off the above mentioned sequence. Depending on the penetration speed of the experiment, n was set to 32 in order to increase signal-to-noise increasing the measurement time to 3.2 ms. By using different echoes of the sequence to generate a single profile, the signal-to-noise can be improved. Using this method, the averaging repetition of a conventional NMR sequence is avoided and circumventing waiting 3 times $T1$ between every measurement. This effectively results in averaging every echo time (50 μs) leading to a 1.6-ms ($n = 16$) or 3.2-ms ($n = 32$) total acquisition time to measure a single liquid profile. The obtained profiles were normalized with a reference measurement performed on a 0.1-M $CuSO_4$ solution to compensate for the coil sensitivity. Finally, to lower signal-to-noise, individual points were time averaged but not averaged over different positions which by consequence leaves the resolution unchanged. Displayed in Fig. 1 is a schematic representation of the setup. The sample lies directly above the rf coil which has a diameter of 4 mm, corresponding to the sensitive region [18]. Last, the setup used a mounted Hamilton microsyringe to generate microliter droplets that fall on top of a porous sample. To cover a range of viscosity, a water-glycerol mixture was used. The composition of the liquids and their physical parameters are shown in Table I. The porous materials used in this study are Whatman nylon-6,6 membranes and Mondi Niveus Top printing paper. The Whatman nylon-6,6 membranes have two different pore diameters, 0.42 μm and 0.53 μm and a thickness of 165 μm. The porosity of the membranes were 0.62 and 0.67, respectively. Both porosity and pore diameter were measured using mercury intrusion porosimetry (MIP). The Mondi Niveus Top printing paper is an uncoated paper with a pore radius of 4 μm, thickness of 90 μm, and weight of 80 gsm. To start the experiment, a microliter-sized droplet is jetted from the syringe. When the droplet reaches the top of the nylon sample, it starts to penetrate the porous media. Liquid profiles were measured for all water glycerol mixtures in both nylon substrates. The 1D liquid profiles from a 50-wt % glycerol mixture penetrating the 0.42-μm pore diameter nylon membrane are shown in Fig. 2. The top of the nylon membrane, determined experimentally, is set to the zero position and liquid profiles are taken every 25 ms. In blue, the liquid profile is shown just before the droplet falls on the nylon membrane. As time progresses, the liquid penetrates into the nylon membrane, indicated by the black arrow. The penetration continues until the liquid reaches the bottom of the membrane at 165 μm. The signal intensity after complete filling is 0.63, which agrees with the porosity of the sample as determined by MIP. The low signal-to-noise ratio of the experiments causes the undulations observed in the maximum signal intensity of the liquid profiles. The profiles in Fig. 2 reveal that also on micrometer scale the liquid penetrates with a sharp moving front inside the porous media. From these liquid profiles, the front position (l[m]) is taken at the position where the liquid signal is around 50% of its saturation level. This exact point is calculated by interpolating the two nearest measurements points. Some deviations may still occur due to the spatial resolution of the measurements points (14.5 μm).

To describe front progress shown in Fig. 2, we adopted a sharp front formalism in combination with Darcy's law. Assuming an incompressible liquid, the fluid flow can be

TABLE I. Physical properties of water-glycerol mixtures used in this study.

Mixture composition water:glycerol (wt %)	Viscosity η (mPa s)	Surface tension σ (mN/N)
100:0	0.89	72.3
75:25	1.89	70.7
50:50	5.38	68.5
30:70	20	66.1

described by three-dimensional (3D) mass conservation with $\nabla \cdot \boldsymbol{q} = \nabla^2, P = 0$ [8], where $\boldsymbol{q}[\mathrm{m}^2/\mathrm{s}]$ represents the fluid flux through the porous media, described by Darcy's law [8],

$$\boldsymbol{q} = \frac{-k}{\eta}\nabla P \tag{1}$$

with $k[\mathrm{m}^2]$ the permeability, $\eta[\mathrm{Pa\,s}]$ the viscosity, and $P[\mathrm{Pa}]$ the pressure. Because the pressure gradient scales with liquid penetration, we will compare the pressure gradients in all directions. As the main pressure component in spontaneous imbibition is the capillary pressure P_c, the maximum pressure drop P observed in any direction should be similar to P_c. P_c can be described by the Young-Laplace equation for capillary pressure,

$$P_c = \frac{2\sigma\cos(\theta)}{r}, \tag{2}$$

where $r[\mathrm{m}]$ is the pore radius, $\sigma[\mathrm{N/m}]$ is the surface tension, and $\theta[^\circ]$ is the liquid-surface contact angle. After using cylindrical coordinates and leaving out the angular coordinate, because the droplet is axisymmetric, we obtain

$$\nabla^2 P = \frac{1}{R^2}\frac{1}{r'}\frac{\partial}{\partial r'}r'\left(\frac{\partial P}{\partial r'}\right) + \frac{1}{l^2}\frac{\partial^2 P}{\partial z'^2} = 0, \tag{3}$$

where we have introduced normalized coordinates $r' = r/R$ and $z' = z/l$ with the droplet radius $R[\mathrm{m}]$ and nylon thickness l. After rewriting this expression, we end up with

$$\epsilon\frac{1}{r'}\frac{\partial}{\partial r'}r'\left(\frac{\partial P}{\partial r'}\right) + \frac{\partial^2 P}{\partial z'^2} = 0, \tag{4}$$

where $\epsilon = (l/R)^2$. From Eq. (4), it becomes clear that the problem can be assumed 1D when the following condition is met: $\epsilon \ll 1$. By comparing the typical droplet radius (2 mm) and the nylon thickness (165 μm), ϵ can be estimated to be 0.0068, showing that the process can be considered as a 1D process. The same condition also holds for paper with a thickness of 90 μm.

Now that we have proven that the liquid penetration in the setup can be assumed to be 1D, we are able to compare our results to 1D models found in literature. Assuming a homogeneous porous structure, the imbibition of the liquid front l can be described according to Darcy's law in one dimension [19], where a constant and isotropic permeability $K[\mathrm{m}^2]$ is assumed throughout the sample. Using the capillary pressure [Eq. (2)] and the following scaling relation for permeability in function of the pore radius $K = K_0 r^2$ [20], an expression for the imbibition front in one dimension is obtained [8],

$$l(t)^2 = \frac{4K_0\cos(\theta)}{\phi}\frac{\sigma r t}{\eta} \tag{5}$$

with $\phi[\%]$, the porosity of the substrate. To test the Darcy scaling with surface tension σ, pore radius r, and viscosity η, imbibition experiments were carried out with different water-glycerol mixtures and nylon membranes with two different pore diameters (0.42 and 0.53 μm). The front positions are determined as described in Fig. 2. Results are shown in Fig. 3, where the front position is plotted as a function of the square root of time. For all different viscosities and pore radii, a linear behavior between l and $\sqrt{t}$ is observed.

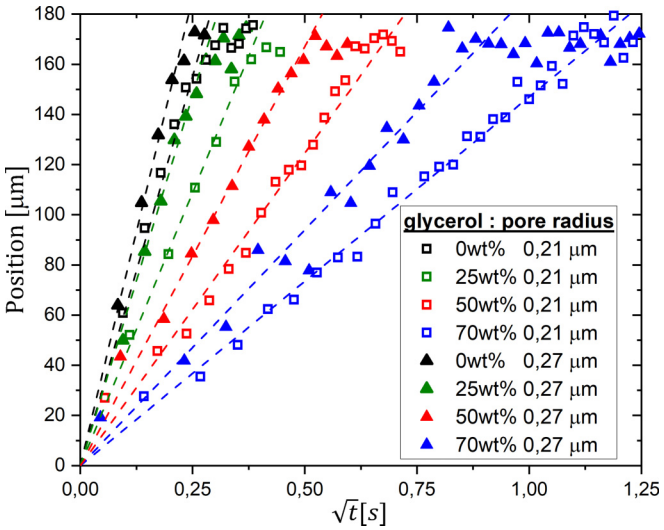

FIG. 3. Imbibition experiments for different water-glycerol mixtures (0, 25, 50, and 75 wt % glycerol) in nylon membranes with different pore radius ($r = 0.21$ μm and $r = 0.27$ μm). The legend gives the amount of glycerol in wt % and the pore radius of the nylon membranes in μm. The fluid front position is given as a function of $\sqrt{t}$.

The experiments stop at $l = 165$ μm, where the end of the membrane is reached. For both pore radii, the rate of penetration slows down with increasing glycerol concentration. In addition, a smaller pore radius leads to a slower imbibition at similar glycerol water ratios. To validate the predicted scaling by Darcy's law [Eq. (5)], the penetration fronts are plotted as a function of rescaled time $\sqrt{\sigma r/\eta}\sqrt{t}[\mathrm{mm}]$, Fig. 4. After rescaling, the absorption measurements coincide on a single master curve. Because other scaling parameters like the permeability and porosity are media dependent, this indicates that the dependency on viscosity and surface tension are correct.

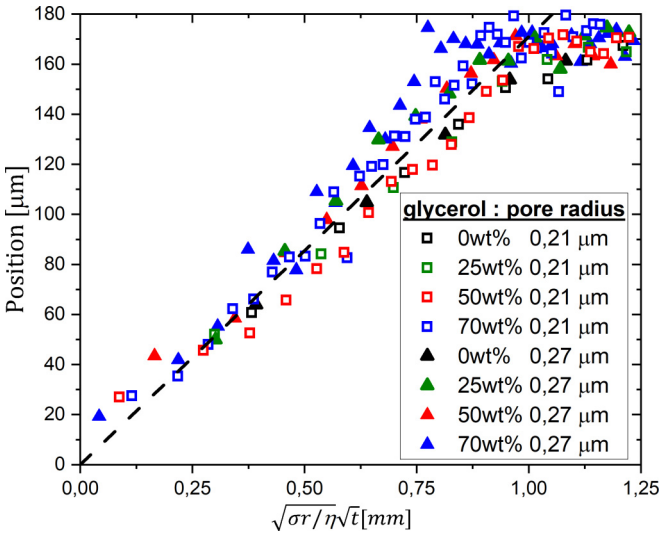

FIG. 4. The liquid penetration depth as function of the rescaled time for the different water-glycerol mixtures (0, 25, 50, and 75 wt % glycerol) in nylon membranes with different pore radii ($r = 0.21$ μm and $r = 0.27$ μm) membranes.

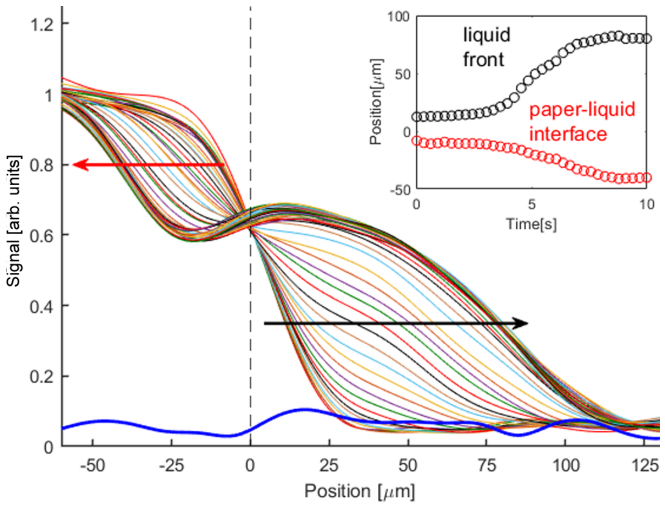

FIG. 5. Liquid profiles for a 0.25-M $CuSO_4$ solution in Mondi Niveus Top printing paper. For clarity, the initial paper-liquid interface at position 0 μm is marked with a dashed line. Shown in top right are the liquid front (black) and swelling front paper-liquid interface (red) indicated by arrows in the main figure. In blue, the signal acquired just before the droplet hits the sample surface is shown.

The corresponding slope of the master curve, being 170, can be used to estimate the dimensionless permeability K_0. When using a typical contact angle for water on nylon-6,6 of 70° [21] and the according porosity, K_0 was calculated to be 0.016 and 0.018 for the 0.43- and 0.53-μm pore diameters, respectively. This value is in good agreement with values found in Tomadakis *et al.* [22], who summarized values for the dimensionless permeability in function of porosity, calculated from different models and experimental results.

Measuring these profiles allows us to investigate physical phenomena with spatial resolution. To illustrate the capability of the measurement technique, imbibition experiments with a Top printing paper (Mondi Niveus) were measured. Profiles where taken every 0.3 s with a 0.25-M $CuSO_4$ solution and can be seen in Fig. 5. In blue, the signal acquired just before the droplet hits the sample surface is shown. In the beginning of the experiment, the paper-liquid interface situates at position 0, marked with a dashed line in Fig. 5. The initial paper position ranges 0–100 μm and has a maximum intensity of 0.6 due to the porosity of paper. Positions above the paper have a signal intensity of 1 and are taken up by the droplet. The first liquid profiles overlap indicating a retardation in the fluid front which was not observed in nylon-6,6. After this retardation, the liquid starts to penetrate inside the paper indicated by the black arrow. The measurement also revealed a swelling front of the paper (red arrow in Fig. 5) that could be measured over time. A corresponding front versus time graph for swelling (red) and penetration (black) is shown on the top right of Fig. 5. From this figure, it can be clearly observed that a retardation period is followed by a period of penetration. The retardation is probably the effect of sizing, a technique commonly used in paper to provide resistance against penetration of liquids [23]. Mondi Niveus Top printing paper has a high amount of AKD sizing which can clarify the retardation. However, further studies are required to investigate this relationship. When comparing swelling with penetration it can be concluded that in the case of water, the swelling front and penetration front will start at almost the same time, around 3 min. The liquid profiles during penetration are less sharp then the ones found in nylon-6,6. This can be easily viewed when comparing the profiles from Figs. 2 and 5 where in the printing paper it can be observed that liquid fronts span the whole width of the sample while in the nylon-6,6 this is not the case. From the last experiment, it can be concluded that liquid penetration in paper is a much more complex processes where swelling, broader liquid fronts, and retardation in uptake are observed. Explaining these phenomena requires further research but lies beyond the scope of this Letter.

In this study, we developed a high-speed NMR technique able to measure the liquid penetration in thin porous media with a time resolution of 10 ms and a spatial resolution of 14.5 μm. We demonstrated that this technique can be used to measure liquid profiles inside nontransparent thin porous media from which penetration behavior can be studied. The measurements revealed that for the nylon-6,6 and water-glycerol mixtures, imbibition at this scale happens with a sharp moving liquid front. The liquid front position for different water-glycerol mixtures varied with the square root of time and could be described by a 1D-Darcy model for capillary action. It was shown that in this medium the Darcy scaling with viscosity, surface tension, and pore radius could be observed at this particular time and length scale. Using this model, the dimensionless permeability of the nylon samples were calculated, which agreed well with values found in the literature. Last, measurements in paper revealed deviations from this 1D-Darcy law, a retardation in uptake, broader fluid fronts, and the occurrence of swelling. The high spatial and time resolution of this technique allows us to study the liquid penetration process in thin nontransparent porous media at small time and length scales.

We acknowledge H. Dalderop (TU/e) and J. Noijen (TU/e) for their support regarding the setup and sample preparation. The authors would like to thank P. Lipman (TU/e) for doing the MIP measurements. This publication is part of the project PQP (Print Quality and Particles) (Project No. 17099) of the research collaboration program High Tech Systemen en Materialen (HTSM) 2018 TTW, which was (partly) financed by the Dutch Research Council (NWO). Last we would like to thank DSM and Canon Production Printing for their support.

[1] S. Krainer, C. Smit, and U. Hirn, The effect of viscosity and surface tension on inkjet printed picoliter dots, RSC Adv. **9**, 31708 (2019).

[2] A. Genbach, N. Jamankulova, I. Iliev, and A. Terziev, Study of fragile capillary-porous coatings in power installations, E3S Web Conf. **85**, 05002 (2019).

[3] H. A. Fadel, Water treatment by fabric capillary action: New technique with ancient origins, J. Am. Water Works Assoc. **106**, 44 (2014).

[4] S.-H. Moon and G. Hwang, Development of the micro capillary pumped loop for electronic cooling, in *2007 13th International Workshop on Thermal Investigation of ICs and Systems (THERMINIC)* (IEEE, 2007), pp. 72–76.

[5] W. W. Wits, R. Legtenberg, and J. H. Mannak, Selecting capillary structures for heat pipes in multilayer printed circuit boards, in *Proceedings of the 5th European Thermal-Sciences Conference (Eurotherm)* (Eindhoven University of Technology, Eindhoven, The Netherlands, 2008).

[6] J. Schoelkopf, P. A. Gane, C. J. Ridgway, and G. P. Matthews, Practical observation of deviation from Lucas–Washburn scaling in porous media, Colloids Surf., A **206**, 445 (2002).

[7] J. Fabricius, J. G. I. Hellström, T. S. Lundström, E. Miroshnikova, and P. Wall, Darcy's law for flow in a periodic thin porous medium confined between two parallel plates, Transp. Porous Media **115**, 473 (2016).

[8] C. Kuijpers, T. van Stiphout, H. Huinink, N. Tomozeiu, S. Erich, and O. Adan, Quantitative measurements of capillary absorption in thin porous media by the automatic scanning absorptometer, Chem. Eng. Sci. **178**, 70 (2018).

[9] M. Kvick, D. M. Martinez, D. R. Hewitt, and N. J. Balmforth, Imbibition with swelling: Capillary rise in thin deformable porous media, Phys. Rev. Fluids **2**, 074001 (2017).

[10] R. Masoodi and K. M. Pillai, Darcy's law-based model for wicking in paper-like swelling porous media, AIChE J. **56**, 2257 (2010).

[11] A. Clarke, T. Blake, K. Carruthers, and A. Woodward, Spreading and imbibition of liquid droplets on porous surfaces, Langmuir **18**, 2980 (2002).

[12] S. Gruener and P. Huber, Capillarity-driven oil flow in nanopores: Darcy scale analysis of Lucas–Washburn imbibition dynamics, Transp. Porous Media **126**, 599 (2019).

[13] C. Kuijpers, H. Huinink, N. Tomozeiu, S. Erich, and O. Adan, Sorption of water-glycerol mixtures in porous Al_2O_3 studied with NMR imaging, Chem. Eng. Sci. **173**, 218 (2017).

[14] P. Glover, P. Aptaker, J. Bowler, E. Ciampi, and P. McDonald, A novel high-gradient permanent magnet for the profiling of planar films and coatings, J. Magn. Reson. **139**, 90 (1999).

[15] E. Ostroff and J. Waugh, Multiple Spin Echoes and Spin Locking in Solids, Phys. Rev. Lett. **16**, 1097 (1966).

[16] P. J. McDonald and B. Newling, Stray field magnetic resonance imaging, Rep. Prog. Phys. **61**, 1441 (1998).

[17] B. Blumich, *NMR Imaging of Materials* (Oxford University Press, Oxford, 2000).

[18] S. J. Erich, J. Laven, L. Pel, H. P. Huinink, and K. Kopinga, Influence of catalyst type on the curing process and network structure of alkyd coatings, Polymer **47**, 1141 (2006).

[19] H. Huinink, *Fluids in Porous Media* (Morgan & Claypool Publishers, 2016).

[20] J. B. Walsh and W. Brace, The effect of pressure on porosity and the transport properties of rock, J. Geophys. Res.: Solid Earth **89**, 9425 (1984).

[21] D. K. Owens and R. Wendt, Estimation of the surface free energy of polymers, J. Appl. Polym. Sci. **13**, 1741 (1969).

[22] M. M. Tomadakis and T. J. Robertson, Viscous permeability of random fiber structures: comparison of electrical and diffusional estimates with experimental and analytical results, J. Compos. Mater. **39**, 163 (2005).

[23] H. L. Lee, J. Y. Shin, C. H. Koh, H. Ryu, D. J. Lee, and C. Sohn, Surface sizing with cationic starch: Its effect on paper quality and papermaking process, Tappi J. **1**, 34 (2002).